An Adaptive Artificial Immune Network for Supervised Classification of Multi-/Hyperspectral Remote Sensing Imagery

Yanfei Zhong, *Member, IEEE*, and Liangpei Zhang, *Senior Member, IEEE*

***Abstract*—The artificial immune network (AIN), a computational intelligence model based on artificial immune systems inspired by the vertebrate immune system, has been widely utilized for pattern recognition and data analysis. However, due to the inherent complexity of current AIN models, their application to multi-/hyperspectral remote sensing image classification has been severely restricted. This paper presents a novel supervised AIN—namely, the artificial antibody network (ABNet), based on immune network theory—aimed at performing multi-/hyperspectral image classification. To construct the ABNet, the artificial antibody population (AB) model was utilized. AB is the set of antibodies where each antibody (ab) has two attributes—its center vector and recognizing radius—thus each ab can recognize all antigens within its recognizing radius. In contrast to the traditional AIN model, ABNet can adaptively obtain these two parameters by evolving the antigens without relying on user-defined parameters in the training step. During the process of training, to enlarge the recognizing range, the immune operators (such as clone, mutation, and selection) were used to enhance the AB model to find better antibody in the feature space, which may recognize as much antigen as possible. After the training process, the trained ABNet was utilized to classify the remote sensing image, exhibiting superior learning abilities. Three experiments with different types of images were performed to evaluate the performance of the proposed algorithm in comparison to other supervised classification algorithms: minimum distance, Gaussian maximum likelihood, back-propagation neural network, and our previously developed artificial immune classifiers—resource-limited classification of remote sensing image and multiple-valued immune network classifier. The experimental results demonstrate that ABNet has remarkable recognizing accuracy and ability to provide effective classification for multi-/hyperspectral remote sensing imagery, superior to other methods.**

***Index Terms*—Artificial immune systems (AISs), image classification, pattern recognition, remote sensing.**

Manuscript received November 16, 2009; revised January 14, 2011; accepted June 27, 2011. Date of publication August 18, 2011; date of current version February 24, 2012. This work was supported in part by the National Basic Research Program of China (973 Program) under Grant 2011CB707105, by the 863 High Technology Program of the People's Republic of China under Grant 2009AA12Z114, by the National Natural Science Foundation of China under Grants 40901213 and 40930532, by the Foundation for the Author of National Excellent Doctoral Dissertation of P.R. China under Grant 201052, by the Program for New Century Excellent Talents in University under Grant NECT-10-0624, and by the Fundamental Research Funds for the Central Universities under Grant 3103006.

The authors are with the State Key Laboratory of Information Engineering in Surveying, Mapping and Remote Sensing, Wuhan University, Wuhan 430079, China (e-mail: zhongyanfei@lmars.whu.edu.cn; zlp62@public.wh.hb.cn).

Color versions of one or more of the figures in this paper are available online at http://ieeexplore.ieee.org.

Digital Object Identifier 10.1109/TGRS.2011.2162589

I. Introduction

IMAGE CLASSIFICATION is an important issue in remote sensing and other applications [1]. The accurate classification of remote sensing images has a wide range of uses, including reconnaissance, assessment of environmental damage, land use monitoring, urban planning, and growth regulation [2]. A major distinction in image classification separates supervised from unsupervised classification methods. Supervised classification permits higher classification accuracy to be achieved owing to the exploitation of training samples during the learning phase, compared to unsupervised classification. In the literature on remote sensing, a variety of different supervised classification algorithms have been designed and implemented based on statistical and computational intelligence frameworks [2], [3] in the past, such as parallelepiped [2], minimum distance (MD) [4], Gaussian maximum likelihood (GML) [4], Mahalanobis distance [5], spectral angle mapper (SAM) [6], the k-nearest neighbor [2], [7], decision trees [8], [9], artificial neural networks [10]–[13], the classifiers based on genetic algorithms [14] or ant colony algorithm [15], and the recently developed support vector machine classifier [16]–[18].

In recent years, a new intelligence theory—artificial immune systems (AISs) [19], [20]—has also been applied to unsupervised and supervised classification of multi-/hyperspectral remote sensing images [21]–[24]. AISs inspired by their natural counterparts have exhibited the following strengths: immune recognition, reinforced learning, feature extraction, immune memory, diversity and robustness, etc. In addition, they have strong capabilities in pattern recognition by utilizing immunological properties, such as clonal selection and immune memory [25], [26]. Experimental results suggest that these artificial immune classifiers for remote sensing imagery can yield better results than traditional classification algorithms, such as maximum likelihood classifier [23], [24]. However, they often require additional user-defined parameters to update the antibody and memory cell population. For example, the previously developed supervised artificial immune classifier—resource-limited classification of remote sensing image (RLCRSI) [23]—relies on the following user-defined parameters: the stimulation threshold, total resource, and affinity threshold scalar (ATS). The classification results are sensitive to the values of these user-defined parameters; furthermore, experimental data need to be used as a selection criteria for the appropriate values incorporated in different images [23], limiting the application of these artificial immune classifiers.

In this paper, to reduce the number of parameters and improve the intelligence of artificial immune classifiers, an adaptive supervised classification algorithm based on artificial immune network (AIN), namely, an artificial antibody network (ABNet), is proposed to classify multi-/hyperspectral remote sensing imagery. The proposed algorithm is designed to adaptively obtain the antibodies or memory cells and subsequently classify the remote sensing image. Furthermore, in contrast to some previous artificial immune classifiers, which are only based on clonal selection theory and immune memory [22], [23], the proposed classifier utilizes not only the aforementioned immunological properties but also the AIN theory. AIN based on immune network theory [27] is an important and effective model of AISs, including aiNet model [28], AIN (AINE) model [29], and the dynamic AIS model [30]. It has been applied to pattern recognition [31], optimization [32], clustering [33], and multimodal electromagnetic problems [34]. AIN simulates the body's adaptive learning and defense mechanism when exposed to invading pathogens. Based on these underlying biological properties of AINs, the proposed ABNet may be regarded as a self-learning highly robust algorithm for the following reasons.

1) It can adjust itself to the data without any explicit specification of functional or distributional form. ABNet can adaptively adjust and build up the recognizing network that consists of the antibodies. Every antibody (ab) has its center vector and recognizing radius and can recognize all antigens in its recognizing radius. All training samples/antigens in the training procedure will be correctly recognized by ABNet.
2) Fewer user-defined parameters for the underlying model. ABNet reduces the number of the parameters due to its ability to adaptively obtain the center vector and recognizing radius of each antibody by training the samples of interest in each class.
3) ABNet can provide a clear and direct way to construct the classifier no matter how complex the decision boundary. Finally, ABNet outputs the set of antibodies for each class, where each antibody has the corresponding class attributes. The class decision boundary can be clearly obtained by the center vector and the radius of each antibody.

The proposed algorithm has been tested and compared to the traditional algorithms and the previous artificial immune classifiers using three real multi-/hyperspectral remote sensing images acquired by Landsat TM (Thematic Mapper) 7, the Pushbroom Hyperspectral Imager (PHI), and the Airborne visible/Infrared Imaging Spectrometer (AVIRIS). The experimental results demonstrate that the proposed approach can have remarkable classification accuracy. Moreover, it provides a more robust artificial immune classifier with fewer user-defined parameters.

The remaining part of this paper is organized as follows. In Section II, we review the immune network theory. An artificial immune model, namely, the artificial antibody population (AB) model, is presented in Section III. Section IV provides a detailed description of the proposed AIN-based AB model for remote sensing image classification. Section V presents a description of the data sets and analyzes the experimental results. Finally, conclusions are drawn in Section VI.

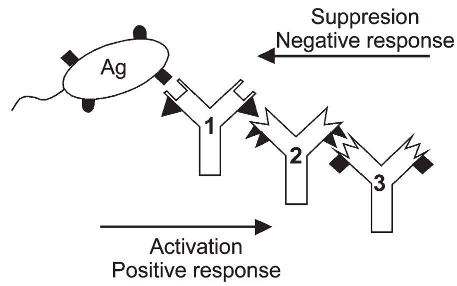

Fig. 1. Immune network principle.

II. AIN

The natural immune system—made up of special cells, proteins, and organs—protects organisms from infection with layered defenses of increasing specificity. In the simplest form, physical barriers prevent pathogens (called antigens ag) such as bacteria and viruses from entering the organism. One type of response is the secretion of antibody (ab) molecules by B cells or B lymphocytes [35]. The clonal selection principle describes the basic characteristics of an adaptive immune response to an antigenic stimulus [36]. When an antigen is detected, the B cells that recognize the antigen with best affinity will proliferate by cloning, where affinity represents the attraction between an antigen and an antibody. During reproduction, the B-cell clones undergo a hypermutation process, whereby the antigen stimulates the B cell to proliferate and mature into terminal antibody-secreting cells—plasma cells. The activated B cells with high antigenic affinities are selected to become memory cells with long life spans. These *memory cells* guarantee a faster response to similar antigens in the future [37].

Immune network theory was proposed by Jerne [38] in an attempt to explain the memory-retention and learning capabilities exhibited by the immune system. Unlike the clonal selection principle, the immune network theory hypothesizes that the immune system maintains a regulated network of cells and molecules that maintain interactions between not only an antibody and an antigen but also the antibodies themselves [32]. If an antigen is recognized by an antibody ab_1, then ab_1 may be recognized by ab_2 and, in turn, ab_2 may be recognized by ab_3, forming a network of antibody interaction (Fig. 1). Recognition among antibodies would elicit a negative response and result in the tolerance and suppression of antibodies. In this way, excessively similar antibodies of the same types will be suppressed to guarantee the appropriate number of antibodies. As a result, the immune system will achieve the final state of stability where these highly adapted antibodies are transformed into long-term memory antibodies. This ensures that memory antibodies can be uniformly distributed in an antigen space. In this way, although there are a relatively small number of antibodies in the immune system, they can cover the entire antigen space and recognize all antigens [32]. These immune network principles will be utilized in this paper.

Based on the immune network theory, several AIN models—aiNet model [28], AIN (AINE) model [29], the dynamic AIS model [30], etc.—have been proposed to successfully solve a wide range of engineering problems [27], such as data analysis and pattern recognition. However, it is difficult to apply current AIN models to remote sensing image classification owing to the huge data volumes associated with remote sensing images, particularly a hyperspectral remote sensing image comprising a large number of bands. Current models require the storage and manipulation of a large network of B cells or antibodies (with the number of B cells or antibodies often exceeding the number of data points), which limits their use even for medium-sized data sets [30]. An excessive number of user-defined parameters in current AIN models are an additional significant drawback.

In our previous work [24], we attempted to solve the aforementioned stated problems by proposing the multiple-valued immune network classifier (MVINC) based on the set of multiple characteristics of multispectral remote sensing image classification. MVINC builds up an immune network composed of three layers—the antigen, the B cell, and the T cell layer—by analogy with the interaction between B cells and T cells in the immune system. When inputting an antigen, MVINC produces the weighing vector to describe the stimulation level of an input antigen pattern to different T cells. Subsequently, by applying a function modified in real time, MVINC produces the feedback vector from T cell to B cell layer to update the network, called the memory pattern or multiple-valued memory pattern. MVINC constantly trains the immune network to the samples of regions of interest (ROIs) using the aforementioned process, until the maximum recorded error is within the tolerance threshold ρ. During the classification process, MVINC learns to classify inputs based on a multiple set of characteristics from 0 to $(m-1)$—indicating the extent to which each one is present—where m represents the total number of characteristics. For the classification of multispectral imagery, m can be replaced with the maximum grayscale value of the image (e.g., $m = 255$). It was noted that the number of the B cell layers is equal to the number of the bands, while the number of the T cell layers corresponds to the number of the classes, implying that each class has only one T cell. This is in keeping with the previous experiments suggesting that MVINC may obtain better classification results for multispectral remote sensing images by utilizing one T cell for each class. However, as the number of hyperspectral remote sensing image bands is greater than the number of spectra in multispectral remote sensing image, complexity of data MVINC has to process is further increased. The quality of MVINC-classified results depends on the T cells; hence, using one T cell to represent one class is rarely optimal. This may lead to the unsatisfactory results.

To utilize the immune network theory and overcome the shortcomings of current immune network models, this paper proposes an adaptive AIN model for multi-/hyperspectral remote sensing image classification.

III. AB Model

To construct the adaptive AIN—ABNet—the AB model was used as its basic component. In our previous work, the use of

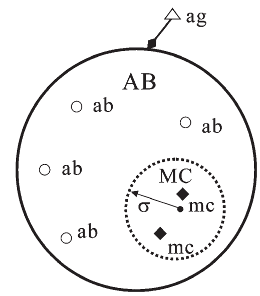

Fig. 2. AB model.

AB model to build up an unsupervised artificial immune classifier (UAIC) for multi-/hyperspectral remote sensing imagery has been proposed [22]. As shown in Fig. 2, the AB model describes the antibody population in immune systems comprising memory cells (denoted by mc) and several antibodies of the same class (denoted by ab). In the AB model, σ represents the AB's scale/radius of influence. For remote sensing image classification, σ determines the recognizing range of the AB, whereby AB recognizes all antigens within the radius σ. Although UAIC may yield satisfactory classification results by using the AB model based on distance threshold and distance threshold scalar (DTS) in [22], the learning and recognizing capacity of UAIC is sensitive to the value of DTS. Different values of DTS may require different computational resources and, thus, may provide different classification results.

In this paper, to simplify the complexity of the model and decrease the user-defined parameters, the concept of memory cells will not be used. The proposed approach directly utilizes the center vector of AB to represent immune memory. According to the principles of AIN (Section II) and the AB model [22], each antibody (ab) should be able to recognize a large number of antigens within its recognizing range. To describe the antibody ab, two attributes of AB are also extended to each single antibody (ab). Every ab is designed to consist of two important attributes: its center vector W and recognizing radius σ; thus, ab can recognize antigens within its recognizing radius. The recognizing radius and center vector of the AB are determined by the set of all individual antibodies (ab) according to the following steps.

To represent the recognizing relationship between antigen (ag) and antibody (ab) in the AB model, the relation function $f(ag, ab)$ was used [39]

$$ag.r = f(ag.V, ab.W) = \begin{cases} 1, & WV^{\mathrm{T}} - \sigma > 0 \\ 0, & \text{otherwise} \end{cases} \tag{1}$$

where $ag.r$ is the recognizing attribute of the antigen, $ab.W$ is the ab center vector, $ag.V$ represents the feature vector of the antigen, σ is the ab recognizing radius, and N_b is the number of image bands. $WV^{\mathrm{T}} - \sigma > 0$ denotes the presence of the antigen in the range of the antibody, i.e., the antigen is recognized by this ab. Hence, $ag.r$ is equal to one; otherwise, the antigen is out of ab recognizing radius, yielding $ag.r$ equal to zero. The fundamental idea is shown in Fig. 3.

Using the aforementioned notations, a set of ab, AB_c, in AIN for the class c, may be constructed, which will recognize all training samples belonging to the particular class c only. In

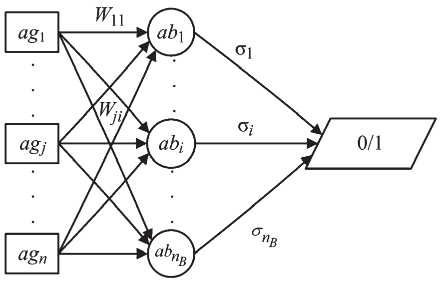

Fig. 3. ABNet (n and n_B represent the number of antigens and antibodies, respectively).

the testing stage, the ABNet determines an antigen's class by selecting the class whose corresponding AB_c recognizes the antigen.

According to the AB model, the antibodies belong to the same immune feature space, which is the spectral space in remote sensing image classification. In the preprocessing, each ab and corresponding ag are projected to the same space with the same vector length. Normalization as a common method transforms the input vector into a unit vector by dividing all components by its original length, but it reduces the original N_b-dimensional feature space to $(N_b - 1)$-dimensional feature space. The following projection process may be used to initialize the antibodies and antigens. Assume that the domain of the antibody input center vector is a bounded set D of the N_b-dimensional space and that S^{N_b} represents N_b-dimensional antibody (ab) of the $(N_b + 1)$-dimensional feature space [40]. To obtain the equal length of the center vector of each antibody with all input information included, we define a transformation $F : D \to S^{N_b}$, where $W \in D$ represents the center vector of the antibody ab as follows [40]:

$$F(W) = \left(W, \sqrt{d^2 - |W|^2}\right), \qquad d \geq \max\left\{|W|\,|W \in D\right\}. \tag{2}$$

According to (2), all antibodies corresponding to D are projected upward on the sphere space S^{N_b} by transformation function $F(W)$. Accordingly, due to the relationship between the antibodies and antigens, all antigens are also projected onto the same feature space.

IV. ABNet for Supervised Classification of Remote Sensing Images

Based on the AB model, a new AIN, named the ABNet, is developed for the supervised classification of multi-/hyperspectral imagery. Multi-/hyperspectral remote sensing data set $X = \{x^1, x^2, \ldots, x^{N_b}\}^{\mathrm{T}}$ is observed and mapped through N_b bands to a finite rectangular lattice $Q = \{(i,j)) : 1 \leq i \leq N_{\text{row}}, 1 \leq j \leq N_{\text{col}}\}$, where N_{row} and N_{col} represent the numbers of rows and columns, respectively. T denotes the transposition of a matrix.

To clearly describe the aforementioned concepts for remote sensing classification and the relationship between ABNet and remote sensing image, the following notations and definitions are used.

1) Let AB denote the set of antibodies, and let ab represent a single antibody, where $ab \in AB$. In relation to remote sensing classification, AB represents the set of trained class centers whereby each class has the corresponding AB_c. That is, for a given class c, $c \in C = \{1, 2, \ldots, n_c\}$, AB_c is designed to recognize all training samples (antigens) belonging to the cth class, where n_c represents the number of classes in the data set. Different classes of samples are recognized by different sets of ABs. Thus, $AB = \{AB_1 \cup AB_2 \cup \cdots AB_{n_c}\}$.
2) Each ab has the following attributes: $ab.c$ represents the class attribute, and $AB_c = \{ab|ab.c \equiv c\}$; $ab.\sigma$ is the recognizing radius of this antibody; and $ab.W$ represents the center vector, $ab.W = \{ab.w_1, \ldots, ab.w_{N_b}\}$, where $ab.w_k$ is the value of its center vector in kth bands and N_b is the number of the image bands.
3) Let AG denote the set of antigens, where ag represents a single antigen, thus $ag \in AG$. In the training stage, ag represents the training samples, while in the classification stage, ag describes the classified pixels.
4) Each ag has the following attributes: $ag.c$ represents the attributes of the class; $ag.V$ represents the feature vector of the antigen, $ag.V = \{ag.v_1, \ldots, ab.v_{N_b}\}$, where $ag.v_k$ is the value of kth band; and $ag.r$ is the recognizing attribute of the antigen, whereby $ag.r = 1$ represents the recognized antigen and $ag.r = 0$ describes the antigen not recognized by any of the antibodies (ab).

Fig. 4 shows a simple two-class example in 2-D feature space to illustrate the training process of ABNet. There are two antigen (sample) sets with different classes, AG_1 and AG_2, as training samples, with each set comprising six antigens. Taking AG_1 as example, $AG_1 = \{ag_{ij}|i \equiv 1, j = 1, 2, 3, 4, 5, 6\}$, ABNet selected ab_{11} as the first antibody and obtained its recognizing radius σ_1 by using all unrecognized antigens with the same class and the other antigens with different classes (see Section IV-C in detail). Because ag_{11}, ag_{12}, and ag_{13} are within the range of σ_1, they are recognized by ab_{11} and are signed as the recognized antigens. All recognized antigens will not take part in the next training. The process is continued until all antigens are recognized by the antibody sets. During the process, to recognize all six antigens in the antigen sets, AG_1 and AG_2, new antibodies $ab_{12}, ab_{21}, ab_{22}, ab_{23}$ are also obtained. After the training process, the ABNet is used to classify these unknown/unclassified antigens and determines the antigen's class by selecting a class of artificial antibody that can recognize the antigen within the recognizing radius σ.

To achieve the aforementioned results, the implementation of ABNet includes the following steps:

1) selection and representation of the samples;
2) ABNet preprocessing and initialization;
3) the training of ABNet;
4) remote sensing image classification using trained ABNet.

These steps are detailed as follows.

A. Selection and Representation of the Samples

Based on the characteristics of the remote sensing image (e.g., texture and spectral properties) and application purposes, ROIs representing the expected classes by *a priori* knowledge

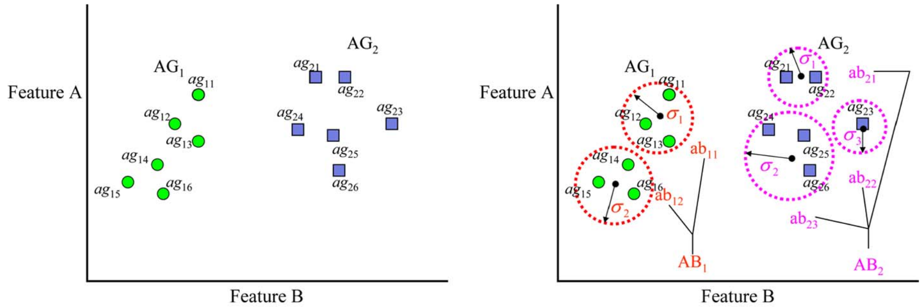

Fig. 4. Training process of ABNet. (a) Two populations of antigens, AG_1 and AG_2. (b) AB_1 and AB_2 recognize all the antigens of the same class, $AB_1 = \{ab_{ij} | i \equiv 1, j = 12\}$ and $AB_2 = \{ab_{ij} | i \equiv 2, j = 1, 2, 3\}$. σ represents the recognizing radius of the corresponding antibody.

can be selected from an image or a spectral library. In the ABNet, the training samples are represented by the set of antigens AG, where ag represents a single antigen, $ag \in AG$. For the supervised classification of a remote sensing image, an antigen represents input training data of the same class. The class attribute of each antigen ag in the remote sensing image is assigned to the class of the corresponding ROI, $ag.c \equiv c \in C = \{1, 2, \ldots, n_c\}$. The number of classes n_c is equal to the number of classes of ROIs obtained in the process.

B. ABNet Preprocessing and Initialization

All antigens are first initialized by normalization using (2). To represent whether the antigen has been recognized by the artificial antibody during the training process, we define the antigen recognizing attribute $ag.r$, using (1), as follows. According to (1), if $ag.r = 1$, the antigen has been recognized by an artificial antibody; otherwise, $ag.r = 0$. At the inception, for any class c, $1 \leq c \leq n_c$, no antigens are recognized, i.e., $ag.r = 0$, $ag \in AG$. That is, each corresponding antibody population AB_c is empty, $n_B^c = 0$, where n_B^c represents the number of the antibodies in AB_c.

C. Training of ABNet

Upon completion of initialization, the ABNet training process commences. For any class c, the following process is repeated until all antigens are recognized by the cth class in AG_c, obtaining the corresponding antibody population AB_c. The training process consists of the following five steps.

Step 1) *Preselection*: Select an antigen as the preselected antigen ag_p, which is closest to the center of ag population with

$$ag_p = \{ag | \arg\min_{ag \in AG_c} Distance(ag, Center), \quad ag.r = 0\} \tag{3}$$

$$Center.v_k = \left(\sum_{j=1}^{n} \sum_{k=1}^{N_b} (ag_j.v_k) \right) / n \tag{4}$$

where the function $Distance()$ uses the Euclidean distance, $Center$ represents the center of ag population, $ag_j.v_k$ is the value of kth bands, and n represents the number of antigens with $ag.r = 0$.

Step 2) *Cloning*: The ag_p is cloned (copied) to obtain a clone set CA, $CA = \{ca_1, \ldots, ca_{n_m}\}$, where n_m is the number of clones generated. The number of clones n_m for each antibody can be adaptively obtained to avoid the impact of variations in the number of clones. The number of clones generated for the preselected antigen ag_p is given by

$$n_m = n \tag{5}$$

where n is the number of the training samples for the cth class.

Step 3) *Mutation*: Each clone feature can be mutated with the probability of mutation assigned, generating a population MU of matured clones, $MU = \{mu_1, \ldots, mu_{n_m}\}$. The mutation process is as follows:

$$mu_i.w_k = ca_i.w_k + p_m \times N(0,1) \times (MAX_k - MIN_k), \quad k = 1, \ldots, N_b; \; i = 1, \ldots, n_m \tag{6}$$

where MAX_k and MIN_k represent the maximum and minimum of the feature vector in kth band; $ca_i.w_k$ and $mu_i.w_k$ represent the values of kth bands in the mutated antibody mu_i and a_i; and $N(0,1)$ is a normally distributed random variable in the range [0,1]. The mutation rate p_m can be adaptively obtained according to the different clones [22] or be set to an experimental value, for example, 0.15.

Step 4) *Adaptive calculation of the new artificial antibody center vector and recognizing radius*. This is the crucial part of the ABNet process. In contrast to the previously developed artificial immune classifier RLCRSI [23], ABNet can adaptively build up the classifier without relying on user-defined parameters.

After the cloning and mutation process is completed, the proposed algorithm will add an artificial antibody ab_j to the ABNet from the mutated population MU, as follows.

1) In the MU population, every matured clone mu_i is known as a candidate artificial antibody with the recognizing radius σ and the center vector W.

To adaptively construct the ABNet, we use the minimum covering principle [40] to obtain σ and W of mu_i as follows:

$$mu_i.W = (mu_i.w_1, \ldots, mu_i.w_k, \ldots, mu_i.w_{N_b}), \quad k = 1, 2, \ldots, N_b \tag{7}$$

$$mu_i.\sigma = (d_1 + d_2)/2 \tag{8}$$

$$d_1 = \max_{ag \notin AG_c} \{\langle mu_i.W, ag.V \rangle\} \tag{9}$$

$$d_2 = \min_{ag \in AG_c} \{\langle mu_i.W, ag.V \rangle > d_1\} \tag{10}$$

where $mu_i.W$ and $mu_i.\sigma$, respectively, represent the center vector and the recognizing radius of a given candidate artificial antibody mu_i, with $mu_i.c \equiv c$. Furthermore, $mu_i.w_k$ represents the value of kth band to mu_i, and $\langle mu_i.W, ag.V \rangle$ denotes the inner product of $mu_i.W$ and $ag.V$. As vectors of all artificial antibodies and antigens are made equal by normalizing using (2), the value of the inner product is sufficient to describe the recognizing capacity of the artificial antibody. The greater the inner product of $mu_i.W$ and $ag.V$, the smaller the distance between mu_i and ag. The recognizing radius of mu_i, $mu_i.\sigma$, can thus be calculated using (8)–(10).

According to the ABNet principles, AB_c should be able to recognize all training samples belonging to the corresponding class c and does not cover any samples of a different class. To satisfy the aforementioned condition, d_1 is used to control the decision boundary, which represents the MD between mu_i and ag in other classes in (9) to prevent other class antigens being trained. That is, $mu_i.c \equiv c$, and the antigens in (9) do not belong to the cth class, $ag \notin AG_c$. In addition, to guarantee recognition of more antigens with the same class for mu_i, d_2 is utilized to find the maximum recognizing radius—equal to the maximum distance between mu_i and ag—where these antigens belong to the same class, $ag \in AG_c$, and the inner product of $mu_i.W$ and $ag.V$ is greater than d_1. By the aforementioned process, the mu_i will recognize as many antigens as possible with the same class.

2) Calculating the number of recognized antigens for each candidate antibody mu_i. All nonrecognized antigens in AG_c are assessed to determine whether they are recognized by the candidate artificial antibody mu_i. If the antigen ag is recognized, $ag.r = 1$; otherwise, $ag.r = 0$. This process can be determined using (1) and is described by the following function:

$$ag.r = \begin{cases} 1 & T \geq 0 \\ 0 & T < 0 \end{cases} \tag{11}$$

$$T = (mu_i.W)(ag.V)^{\mathrm{T}} - mu_i.\sigma. \tag{12}$$

After the completion of the aforementioned process, the number of recognized antigens by mu_i, m_i, is obtained.

3) According to Steps 1) and 2), each candidate artificial antibody has the corresponding number of the recognized antigens m_i. The candidate artificial antibody with the maximum value of m_i becomes a new artificial antibody ab_j and is added to the AIN $n_B^c = n_B^c + 1$, where n_B^c represents the number of antibodies in AB_c. The remaining candidate antibodies become redundant and are consequently removed.

4) The new artificial antibody ab_j is used to recognize the ag with $ag.r = 0$ in AG_c, and the number of recognized antigens m_j by ab_j is recorded.

According to the aforementioned steps, two antibody attributes—the center vector W and the recognizing radius σ—are adaptively obtained by training these nonrecognizing antigens (samples).

Step 5) *Classification of the training samples*: If all antigens in AG_c are recognized, the training process and the building of ABNet on this particular class c are completed, and the artificial antibody set of the cth class AB_c is obtained, $AB_c = \{ab_j | j = 1, \ldots, n_B^c\}$. In this case, the algorithm proceeds to Step 6); otherwise, the process repeats from Steps 1) to 5).

Step 6) *Stopping condition for the training procedure*. If c is equal to the number of classes n_c, the training procedure has been completed. Otherwise, the next class will be trained according to the proposed algorithm from Steps 1) to 6), and $c = c + 1$.

The ABNet is built using the above outlined training procedure. That is, all the sets of artificial antibodies were obtained for all ROIs, $AB = \{AB_1 \cup AB_2 \cup \cdots AB_{n_c}\}$ and $ab \in AB_c = \{ab | ab.c \equiv c\}$, and will be subsequently used in the remote sensing image classification.

D. Classification

Upon completion of the training procedure, the ABNet becomes available for classification. It is worth noting the dual purpose of antigen: In the classification process, the antigen represents the unclassified pixels, whereas during the process of training, it describes the training samples. The ABNet determines an input antigen's class by selecting the class whose corresponding artificial antibody set recognizes the antigen. The classification consists of two steps as follows.

Step 1) When the classified antigen ag is input to the system, ABNet first determines whether the antigen is recognized by the artificial antibody set. If the antigen is recognized by an antibody in AB_c using (11), the antigen is assigned to the cth class, $ag.c = c$. If the antigen cannot be recognized by any of the artificial antibodies, i.e., $ag.c = 0$, then the antigen will be classified in Step 2).

Step 2) The antigen is out of the current antibody population and is not recognized, $ag.c = 0$, in Step1). ABNet

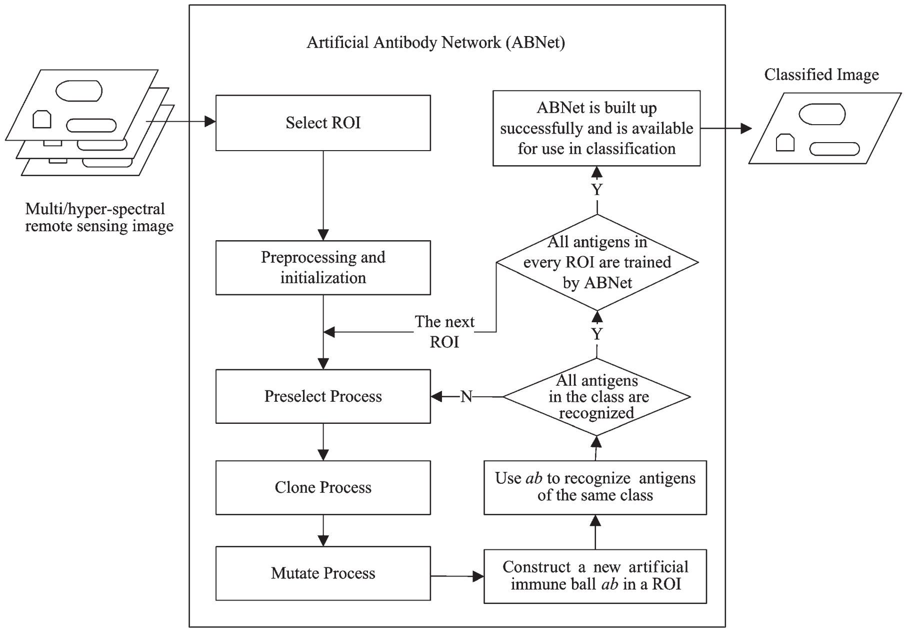

Fig. 5. Flowchart of ABNet.

will calculate the distance between the antigen and the centers of the antibody sets $AB_c.W$ to determine the class of the antigen. Since the proposed algorithm is applied to multi-/hyperspectral remote sensing image classification, the distance between ag and $AB_c.W$ is calculated using the SAM algorithm. Since the SAM algorithm uses only the vector direction and not the vector length [5], [6], this method is insensitive to illumination. The distance function is defined as follows:

$$\begin{aligned} dis(ag, AB_c) &= \alpha \\ &= \cos^{-1}\left[\frac{\sum_{k=1}^{N_b}(ag.v_k)(AB_c.w_k)}{\left[\sum_{k=1}^{N_b}(ag.v_k)^2\right]^{\frac{1}{2}}\left[\sum_{k=1}^{N_b}(AB_c.w_k)^2\right]^{\frac{1}{2}}}\right] \end{aligned} \tag{13}$$

$$AB_c.W = \{AB_c.w_k | k = 1, 2, \ldots, N_b\} \tag{14}$$

where $AB_c.W$ represents the center vector of the cth artificial antibody set calculated by the following function:

$$AB_c.w_k = \sum_{i=1}^{n_B^c}(m_i \times ab_i.v_k) / \sum_{i=1}^{n_B^c} m_i, \qquad ab_i.c \equiv c \tag{15}$$

where m_i is the number of recognized antigens by ab_i (see also Section IV-C-Step-4)-4) and n_B^c represents the number of antibodies in AB_c.

Finally, ABNet outputs the classified multi-/hyperspectral remote sensing image results.

The flowchart for ABNet is shown in Fig. 5.

TABLE I
PARAMETER CONFIGURATIONS OF THE CLASSIFICATION METHODS IN THREE EXPERIMENTS

Methods	Parameters			
MD	None			
GML	None			
BPNN	Experiments	Hidden layers	Learning rate	Momentum rate
	Experiment 1	1	0.2	0.9
	Experiment 2	1	0.25	0.95
	Experiment 3	1	0.15	0.85
MVINC	Experiments	Tolerance threshold ρ		
	Experiment 1	0.15		
	Experiment 2	0.15		
	Experiment 3	0.15		
RLCRSI	Experiments	Stimulation threshold	Total resource	ATS
	Experiment 1	0.85	50	0.8
	Experiment 2	0.85	50	0.8
	Experiment 3	0.85	50	0.8
ABNet	None			

V. Experiments and Analyses

The proposed ABNet and the previous artificial immune classifiers, MVINC and RLCRSI, were implemented using proprietary software written in Visual C++ 6.0 programming language, and the traditional classifiers such as MD, GML, and back-propagation neural network (BPNN) were applied using ENVI software. Three different types of remote sensing images, one multispectral remote sensing (TM) and two hyperspectral remote sensing images (PHI and AVIRIS), were used to evaluate the classification capacity of all classifiers in each experiment, including ABNet, MD, GML, and BPNN, as well as the previously developed artificial immune classifiers RLCRSI [23] and MVINC [24]. The parameter configurations of each classifier for the experiments are listed in Table I, noting the following specific characteristics for each classifier.

1) MD and GML do not need the parameters.
2) The number of hidden layers, the learning rate, momentum rate, and training iterations in BPNN need to be set.

3) In RLCRSI [23], the user-defined parameters, the stimulation threshold, total resource, and ATS need to be set.
4) MVINC is reliant on user-defined tolerance threshold σ parameter.
5) ABNet can adaptively obtain the center vector and recognizing radius and control the number of antibodies.

A. Accuracy Measurement

A quantitative measurement of classification accuracy is used to assess the quality of the image classification using the average accuracy (AA), the overall accuracy (OA), and the Kappa coefficient (Kappa) [5]. AA is the average of the individual class producers' accuracy, and OA is simply the sum of the pixels correctly classified divided by the total number of samples. The resulting quality was assessed for each classification method, using the same testing set of pixels for computing confusion matrix and the accuracy measures.

Prediction rate is defined as the percentage of correctly predicted samples. As the aim is to use a statistical measure to determine if two methods have the same accuracy, McNemar's tests will be used to compare the misclassification rates obtained with different methods in terms of statistical significance in all experiments.

McNemar's test is a direct comparison method for determining the statistical significance of differences observed in two sets of classifications using the same validation set [41]. Given two classifiers C_1 and C_2 (e.g., MVINC and ABNet), null hypothesis is that the two algorithms C_1 and C_2 have the same error rate. This test compares the number of pixels misclassified by C_1, but not by C_2 (M_{12}), with the number of cases misclassified by C_2, but not by C1 (M_{21}). If $M_{12} + M_{21} \geq 20$, the X^2 (where X^2 is defined by (16)) statistics can be considered as following a chi square distribution (with one degree of freedom) [42]

$$X^2 = \frac{(|M_{12} - M_{21}| - 1)^2}{M_{12} + M_{21}} \approx \chi_1^2 \tag{16}$$

and McNemar's test accepts the hypothesis that the two classification algorithms have the same error rate at significance level α if this value is less than or equal to $\chi^2_{\alpha,1}$, for example, $\chi^2_{0.05,1} = 3.841459$ [43]. That is, if McNemar's value X^2 is greater than $\chi^2_{0.05,1}$, the null hypothesis is false, and the two algorithms are significantly different. We applied the McNemar's test to each pair of compared algorithms. The case $M_{12} + M_{21} < 20$ for which the chi square approximation should not be applied [42], [44]. In the following experiments, the case $M_{12} + M_{21} < 20$ does not occur.

In addition to the classification accuracy, the computation time is another important consideration. For the six classifiers (MD, GML, BPNN, MVINC, RLCRSI, and ABNet), the computation times have also been given for the experiments.

B. Experiment 1: Wuhan TM Image

The first experiment was performed using a 30-m-resolution multispectral Landsat TM image (1024 × 1024 pixels) of Wuhan city with six bands, acquired on October 26, 1998 (Fig. 6). The observed image area was expected to consist of six classes: Yangtze River, lake, soil, vegetation, building, and bare land/road. Six ROIs representing the six classes were selected as training regions, and each training region had ground reference sample points. Fig. 7 shows the spectra of the six training regions. The list of classes and the number of labeled samples for each class are given in Table II. All six bands were used for classification. In order to train the algorithms, the training data set—containing approximately half of the available samples—was obtained randomly from the labeled samples.

Fig. 8(a)–(f) shows the classification results using MD, GML, BPNN, MVINC, RLCRSI, and ABNet, respectively. To evaluate the classification accuracy, a test field map is shown in Fig. 8(g) based on ground reference data. The visual comparisons of the six supervised classifications in Fig. 8 show varying degrees of accuracy in pixel assignment. The six classifiers

Fig. 6. Wuhan TM image, October 1998 RGB (3,2,1).

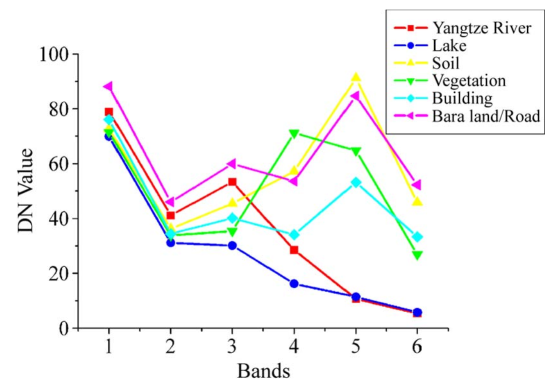

Fig. 7. Spectra of six classes.

TABLE II
LIST OF CLASSES AND NUMBER OF LABELED SAMPLES IN EACH CLASS FOR EXPERIMENT 1

Class Name	Number of labeled samples
Yangtze River	6811
Lake	10486
Soil	4034
Vegetation	10890
Building	7325
Bare land/Road	7173
Total number of samples	46719

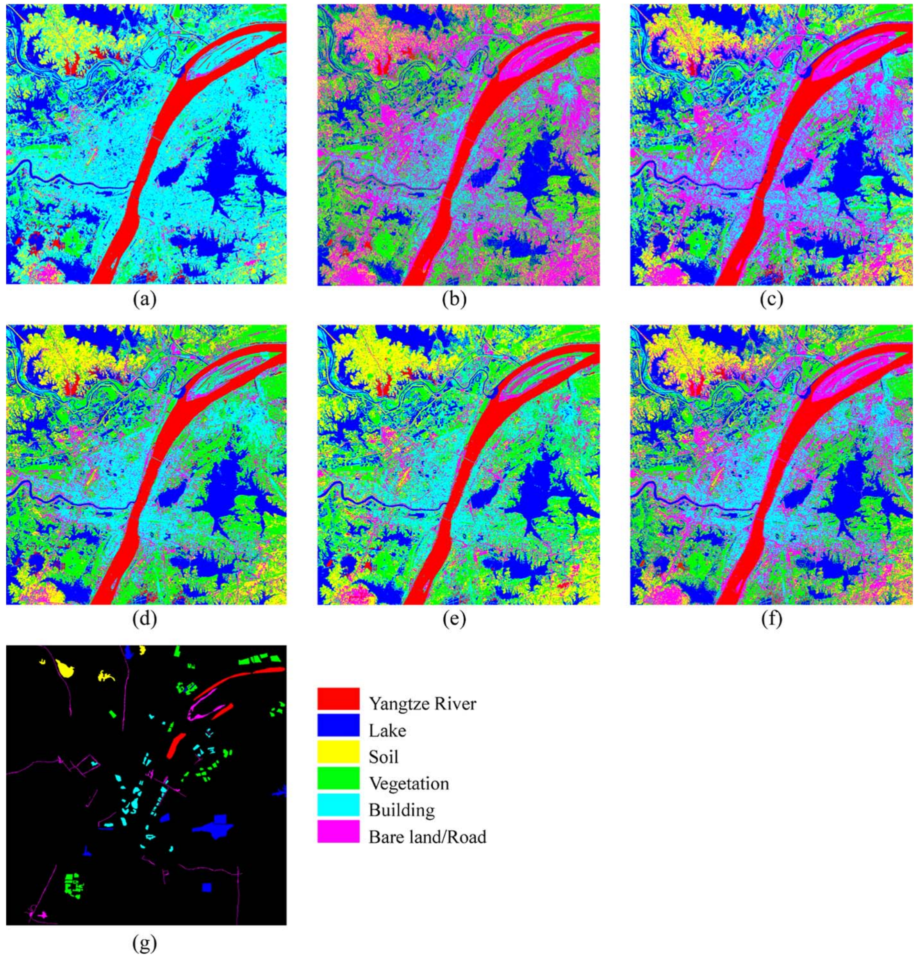

Fig. 8. Supervised classification images for Wuhan TM image. (a) MD. (b) Maximum likelihood. (c) BPNN. (d) MVINC. (e) RLCRSI. (f) ABNet. (g) Ground reference data.

have similar classification results in the Yangtze River and lake classes. However, it is hard for MD to classify soil as shown in the top left corner of Fig. 8(a). Furthermore, there are many vegetation and bare land/road class pixels misclassified to the building classes using other classifiers. In GML classification results, although the bare land/road class may have better visual results, many other class pixels (building and soil in particular) are also wrongly assigned to this class. Compared to GML, BPNN has significantly improved classification accuracy, but many building pixels are still assigned to the bare land/road class. Regarding the two previously developed artificial immune classifiers—MVINC and RLCRSI—they were found to be competent in their classification, even though some bare land/road pixels were wrongly assigned to building class. As shown in Fig. 8(f), ABNet can achieve the better visual accuracy in not only the vegetation class but also other classes, e.g., building and bare land/road classes.

For a more detailed verification of the results, the overall and per-class accuracies in terms of AA, OA, Kappa, and computational time are presented in Table III for each of the classification methods (MD, GML, BPNN, MVINC, RLCRSI, and ABNet). The best accuracy was highlighted in bold for each row in the table.

As shown in Table III, using any of the classification methods, Yangtz River and lake classes can be recognized at least 96% per-class accuracy. For building and bare land/road classes, six classifiers show different classification capability. GML and BPNN have difficulty recognizing the buildings, whereas they have good classification accuracy to bare land/road class. In contrast, the classification accuracy to the building class using MD, MVINC, and RLCRSI is higher than 85%, compared to under 72% for the bare land/road class. One reason for such low accuracy is that the spectra of building and bare land/road are too similar to these classifiers; thus, only one of the two classes could be recognized correctly. Table III shows that ABNet has the best classification accuracy for not only the building but also bare land/road class. It is worth noting that ABNet did not have the highest classification accuracy for each class; however, it obtained the best OA for the entire set. Hence, it was proven that ABNet is accurate, is able to generalize and produce a well-balanced internal distribution of error, and has better overall classification ability than other classifiers. Regarding computational time, BPNN requires excessive processing time (356.3 s for 300 iterations), while MD is most efficient, taking only 3.1 s. In comparison among three artificial immune classifiers, ABNet has the best classification accuracy of 93.70%, with the reasonable computational time of 18.6 s, an improvement on RLCRSI.

The main reason for the comparatively high accuracy achieved by ABNet is that GML is based on the assumption

TABLE III
COMPARISON OF SIX METHODS OF CLASSIFICATION FOR WUHAN TM IMAGE

Class	MD	GML	BPNN	MVINC	RLCRSI	**ABNet**
Yangtze river	99.52%	98.59%	99.19%	**99.60%**	99.44%	98.22%
Lake	**99.51%**	96.75%	98.75%	99.17%	98.90%	98.70%
Soil	69.66%	45.31%	81.98%	86.17%	**91.25%**	87.16%
Vegetation	70.15%	89.83%	87.55%	**95.62%**	91.89%	94.21%
Building	**96.18%**	61.67%	63.58%	85.41%	85.64%	87.18%
Bare land/Road	49.48%	**91.83%**	90.17%	64.92%	71.53%	91.65%
AA	80.75%	80.66%	86.87%	88.48%	89.78%	**92.85%**
OA	81.89%	84.71%	87.92%	89.87%	90.40%	**93.70%**
Kappa	0.7796	0.8125	0.8527	0.8761	0.8829	**0.9230**
Time	3.1s	4.1s	356.3s	5.5s	23.4s	18.6s

TABLE IV
MCNEMAR'S TEST FOR WUHAN TM IMAGE

Methods (OA)	ABNet (93.70%)	RLCRSI (90.40%)	MVINC (89.87%)	BPNN (87.92%)	GML (84.71%)	MD (81.89%)
ABNet	NA	712.00	785.65	1563.29	2845.64	3842.50
RLCRSI		NA	21.20	264.21	989.39	2409.48
MVINC			NA	129.69	725.43	2089.88
BPNN				NA	359.26	909.78
GML					NA	163.97
MD						NA

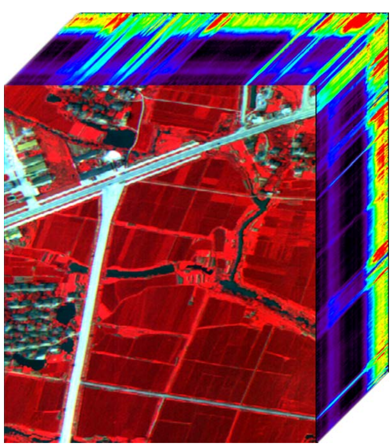

Fig. 9. Xiaqiao PHI image RGB (70,40,10).

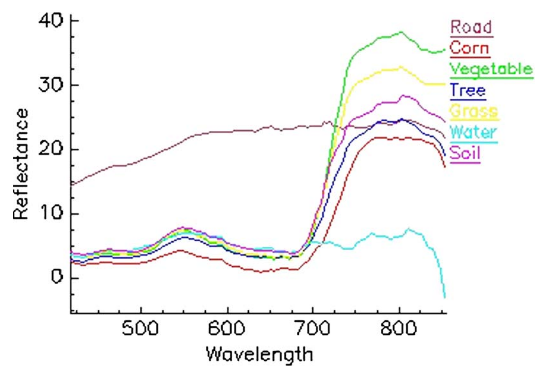

Fig. 10. Spectra of seven land-cover classes.

TABLE V
LAND-COVER CLASSES AND ASSOCIATED NUMBERS OF PIXELS USED IN EXPERIMENT 2

Class Name	Number of labeled samples
Road	716
Corn	1430
Vegetable	1030
Tree	263
Grass	255
Water	492
Soil	585
Total number of samples	4771

that both training data and the classes themselves display multivariate normal (Gaussian) frequency distributions [2]. However, due to the complexity of ground substances and the diversity of disturbance, data from remotely sensed images often do not strictly adhere to this rule which, therefore, leads to the relatively poor performance. BPNN may achieve better accuracy; however, the main drawback to BPNN is the slow learning phase [45]. The selection of the learning rate and momentum rate, usually determined empirically, affects the BPNN convergence. The previous artificial immune classifier RLCRSI may also obtain satisfactory results, but it requires a large number of user-defined parameters to control the memory cells and the classification accuracy, such as the stimulation threshold, total resource, and ATS [23]. In contrast, ABNet decreased the number of user-defined parameters and improved the algorithm intelligence. It is a type of data-driven self-adaptive method that can adjust itself to the data without any explicit specification of functional or distributional form for the underlying model. ABNet adopts an artificial antibody model to adaptively construct the network and obtains two parameters (its center vector and recognizing radius); therefore, it can provide a clear and direct way to construct the classifier and more intelligent classification method, no matter how complex the decision boundary may be. These characteristics enable ABNet to achieve the best accuracy for multispectral image classification.

In addition to the classification accuracy, Table IV provides a pairwise comparison of the six supervised classification algorithms using McNemar's test. McNemar's test is a useful tool to determine if two classification methods have significantly different prediction rates. From Table IV, it can be seen that all values of McNemar's test are greater than the critical value $\chi^2_{(0.05,1)}$ (3.841459). This implies that all classification methods have significantly different prediction rates and ABNet is significantly more accurate than RLCRSI and MVINC. It is worth

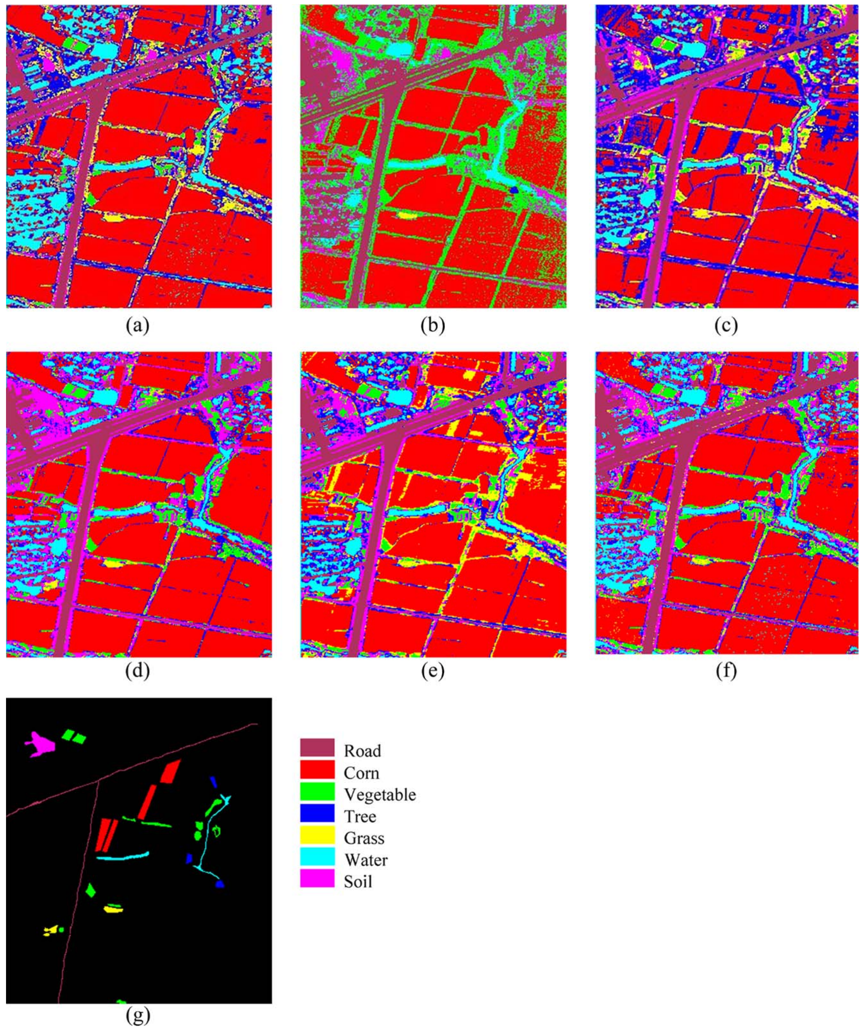

Fig. 11. Supervised classification images for the PHI image. (a) MD. (b) Maximum likelihood. (c) BPNN. (d) MVINC. (e) RLCRSI. (f) ABNet. (g) Ground reference data.

TABLE VI
COMPARISON OF ABNET WITH OTHER ALGORITHMS IN CLASSIFYING THE PHI IMAGE

Class	MD	GML	BPNN	MVINC	RLCRSI	**ABNet**
Road	99.86%	99.72%	100%	**100%**	**100%**	**100%**
Corn	77.41%	89.72%	98.32%	99.16%	98.81%	**99.23%**
Vegetable	65.05%	**98.93%**	84.85%	86.70%	80.10%	93.59%
Tree	80.61%	55.51%	47.15%	54.75%	70.34%	**88.59%**
Grass	**78.43%**	51.76%	38.04%	46.67%	63.92%	71.76%
Water	99.19%	84.76%	99.39%	99.39%	99.80%	**100%**
Soil	61.37%	68.03%	72.99%	83.93%	**86.84%**	85.81%
AA	80.27%	78.35%	77.25%	81.51%	85.69%	**91.28%**
OA	78.62%	86.13%	86.63%	89.50%	90.15%	**94.51%**
Kappa	0.75	0.835	0.8371	0.8696	0.88	**0.9321**
Time	3.8s	8.2s	120.3s	6.3s	15.5s	25.4s

noting that the value of McNemar's test between RLCRSI and MVINC is the lowest (21.20). Although the value is still well above 3.841459, to some extent, it indicates that RLCRSI and MVINC are more similar than other classifiers.

C. Experiment 2: PHI Image

The data set used was acquired from the Xiaqiao test site, a mixed agricultural area in China, using the PHI. In this experiment, 80 bands of the PHI image (340 $\times$ 390 pixels) were used, and their spectral ranges were from 0.417 to 0.854 μm. Fig. 9 shows the experimental PHI image cube. Seven representative classes, namely, road, corn, vegetable, tree, grass, water, and soil, were considered. Fig. 10 shows the reflectance curves of these land-cover classes with the list of classes, while Table V gives the number of labeled samples for each class. All 80 bands were used for classification.

Fig. 11(a)–(e) shows the classification results using MD, GML, BPNN, MVINC, and RLCRSI, respectively. Fig. 11(f) shows the classification result using ABNet. To evaluate the

TABLE VII
McNemar's Test for PHI Image

Methods (OA)	ABNet (94.51%)	RLCRSI (90.15%)	MVINC (89.50%)	BPNN (86.63%)	GML (86.13%)	MD (78.62%)
ABNet	NA	32.23	116.56	242.52	198.25	620.88
RLCRSI		NA	54.63	154.09	103.08	544.69
MVINC			NA	47.30	31.97	345.83
BPNN				NA	0.24	176.69
GML					NA	108.07
MD						NA

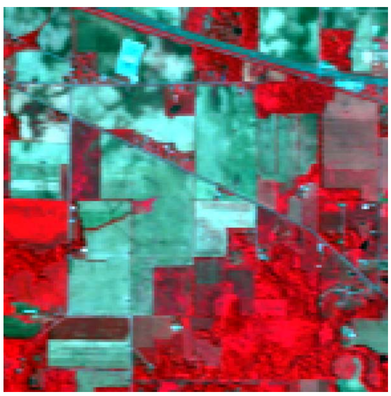

Fig. 12. Indian Pine AVIRIS Image RGB (57,27,17).

TABLE VIII
Land-Cover Classes and Associated Numbers of Pixels Used in Experiment 3

Class Name	Number of labeled samples
C1. Corn-no till	1434
C2. Corn-min till	834
C3. Grass/Pasture	497
C4. Grass/Trees	747
C5. Hay-windrowed	489
C6. Soybeans-no till	968
C7. Soybeans-min till	2468
C8. Soybeans-clean till	614
C9. Woods	1294
C10.Bldg-Grass-Tree drives	380
Overall	9725

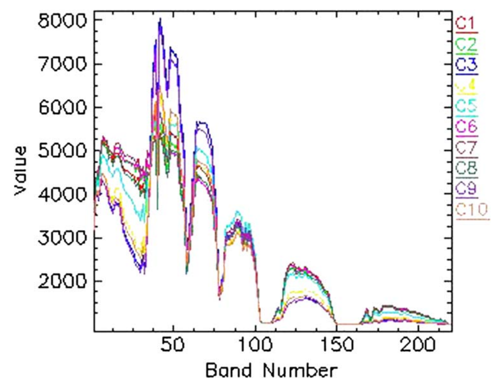

Fig. 13. Spectra of ten land-cover classes.

classification accuracy, a test field map is shown in Fig. 11(g), based on the ground reference data. The training data set, containing approximately half of the available samples, was obtained randomly from the labeled samples. The classification accuracies for the six classifiers are given in Table VI.

As can be seen from Table VI, MD has the highest accuracy for grass class (78.43%), but MD is confused by vegetation, which is assigned to other classes. GML has the best classification accuracy for vegetable class, but the noise affects the overall classification accuracy shown in the right of Fig. 11(b). BPNN requires most computational time (120.3 s) and is confused by trees, with only 47.15% classification accuracy. Two previous artificial immune classifiers have better classification results than traditional classification algorithms, but there are still misclassified pixels with some grass pixels being misclassified as vegetable pixels (Fig. 11(d) and (e). In addition, RLCRSI has better classification accuracy for soil class than MVINC and ABNet. On the whole, although ABNet did not obtain the best accuracy for grass, vegetable, and soil classes, it produces a better overall classification accuracy than other classifiers. It improves the OA from 78.62% to 94.51% (by 15.89%) and the Kappa from 0.75 to 0.9321 (i.e., by 0.1821) with the satisfactory computational time of 25.4 s. McNemar's value is compared to a critical value shown in Table VII; it demonstrates that ABNet is significantly different from other classifiers. These results demonstrate that ABNet is also a better classifier for hyperspectral remote sensing images.

D. Experiment 3: AVIRIS Image

In the previous two experiments, a multispectral TM image with six bands and a hyperspectral PHI image with 80 bands have been tested. To test a hyperspectral image with more bands (> 200), image data with 220 bands were used in this experiment; the image was acquired by the AVIRIS in June 1992 and was downloaded from the Web site (http://dynamo.ecn.purdue.edu/~biehl/MultiSpec). The image data (145×145 pixels) shown in Fig. 12 represent the agricultural area of Indian Pine in the northern part of Indiana and are composed of 220 spectral channels with spectral ranges from 0.417 to 0.854 μm in approximately 10-nm bandwidths [46]. The following ten most representative land-cover classes were considered: Corn-no till (C1), Corn-min till (C2), Grass/Pasture (C3), Grass/Trees (C4), Hay-windrowed (C5), Soybeans-no till (C6), Soybeans-min till (C7), Soybeans-clean till (C8), Woods (C9), and Bldg-Grass-Tree drives (C10). The list of classes and the number of labeled samples for each class are given in Table VIII. Half of the available samples were used to train the classifiers except C10. To avoid the singularity problems of the covariance matrix, the number of the training samples for C10 is equal to 230 to exceed the number of bands. Fig. 13 shows the reflectance of the ten land-cover classes. All 220 bands were used for classification.

The classification images of six classifiers are shown in Fig. 14, while Table IX lists the classification accuracy and computational times of all classifiers. From Fig. 14 and Table IX, it can be seen that the MD classifier is not adapted to classify a hyperspectral image. MD utilizes only the mean value of the training samples to classify the hyperspectral image resulting in misclassification. For example, many Soybeans-min pixels were misclassified to Corn-no till and Soybeans-no till pixels. The GML classifier has the highest classification accuracy for Soybeans-min and Woods classes, 99.35% and

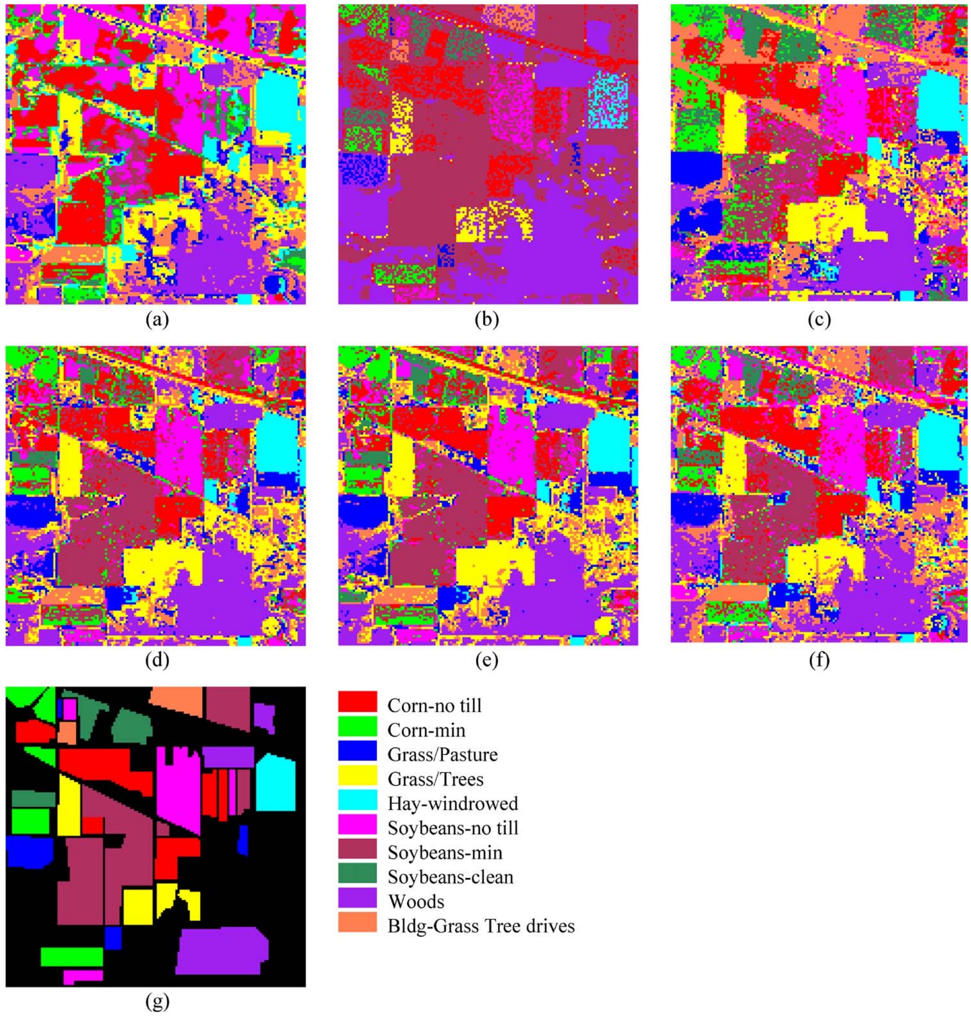

Fig. 14. Supervised classification images for the AVIRIS image. (a) MD. (b) Maximum likelihood. (c) BPNN. (d) MVINC. (e) RLCRSI. (f) ABNet. (g) Ground reference data.

TABLE IX
COMPARISON OF ABNET TO OTHER ALGORITHMS IN CLASSIFYING THE AVIRIS IMAGE

Class	MD	GML	BPNN	MVINC	RLCRSI	**ABNet**
C1. Corn-no till	58.23%	70.78%	81.59%	69.60%	75.17%	**85.91%**
C2. Corn-min till	17.15%	50.48%	65.71%	60.19%	64.99%	**69.42%**
C3. Grass/Pasture	2.82%	50.10%	70.82%	86.92%	89.54%	**91.35%**
C4. Grass/Trees	72.69%	60.37%	95.05%	96.39%	**98.53%**	95.58%
C5. Hay-windrowed	99.39%	50.72%	99.39%	99.39%	99.39%	**99.80%**
C6. Soybeans-no till	47.83%	53.41%	76.34%	81.61%	85.43%	**86.05%**
C7. Soybeans-min till	16.61%	**99.35%**	57.33%	81.48%	84.00%	82.54%
C8. Soybeans-clean till	5.54%	50.00%	81.11%	47.39%	57.98%	**68.08%**
C9. Woods	83.69%	**99.85%**	85.63%	95.90%	96.99%	96.21%
C10.Bldg-Grass-Tree drives	38.68%	60.53%	80.79%	36.32%	47.37%	**80.53%**
AA	44.26%	64.56%	79.38%	75.52%	79.94%	**85.55%**
OA	42.76%	73.85%	75.40%	78.24%	82.04%	**85.41%**
Kappa	0.3520	0.6831	0.7191	0.7463	0.7910	**0.8313**
Time	11.1s	18.3s	1436.7s	30.7s	150.8s	129.3s

99.85%, respectively, while other classes do not have satisfactory results.

To obtain the best possible BPNN result (1436.7 s for 1000 iterations) for this experimental image, the water absorption bands have been discarded first, and the number of bands was reduced by the simple feature selection method considering one band every two. Fig. 14(c) shows the BPNN classification result, and the OA of BPNN is 75.40%. MVINC and RLCRSI may obtain better classification results than traditional classifiers, but there are still some errors; Corn-min pixels are misclassified to Soybeans-min pixels in the bottom left corner. In comparison of Fig. 14(a)–(f) with Fig. 14(g), the classification image of ABNet demonstrates the best visual result for all classes.

TABLE X
McNEMAR'S TEST FOR AVIRIS IMAGE

Methods (OA)	ABNet (85.41%)	RLCRSI (82.04%)	MVINC (78.24%)	BPNN (75.40%)	GML (73.85%)	MD (42.76%)
ABNet	NA	60.96	225.62	356.66	566.04	3840.47
RLCRSI		NA	115.06	153.66	208.86	3208.26
MVINC			NA	25.722	56.17	2713.13
BPNN				NA	5.888	2500.44
GML					NA	1771.72
MD						NA

According to the earlier analysis, the traditional classifiers do not achieve satisfactory classifications of the AVIRIS image. One reason may be that some water absorption bands (104–108, 150–163, 220) influence the classification results. If these bands are excluded, better classification results may be obtained. In addition, as the Hughes phenomenon [47] can be observed in high-dimensional feature spaces, the classification accuracy may also be improved by dimension reduction [48]–[50]. ABNet inherits the biological properties of self-organizing, self-learning, and self-memory to adaptively obtain each artificial antibody during the training process. In the process of classification, ABNet utilizes these antibodies to recognize the image pixels, and each antibody has its corresponding center vector and recognizing radius. Within the range of the recognizing radius, the antibody will recognize the image pixels with the same classes. Although ABNet requires more computational time than MD, GML, and MVINC, it produces better classification results than other classifiers shown in Table IX. The specific improvements are as follows: ABNet improved overall classification accuracy from 42.76% to 85.41% (an improvement of 42.65%) and the Kappa from 0.3520 to 0.8313 (an improvement of 0.4793). McNemar's value is compared to a critical value shown in Table X. It describes that ABNet is significantly different compared to other classifiers, as the values are greater than the critical value $\chi^2_{(0.05,1)}$ (3.841459). As discussed in this experiment, ABNet is an effective classifier to apply with hyperspectral remote sensing imagery.

VI. CONCLUSION

A novel supervised algorithm based on the immune network theory, ABNet, was designed and implemented for classifications of multi-/hyperspectral remote sensing images. To construct the ABNet, the concept and model of artificial antibody (AB) was proposed based on immune network theory and previous work. According to the model, every AB has two important attributes, its center vector and recognizing radius. Within the range of the recognizing radius, all antigens can be recognized by the AB. During the course of training, the sets of AB corresponding to every class were adaptively obtained by training all antigens, i.e., the recognizing radius and center vector of every AB were determined. At the same time, ABNet was built up successfully by utilizing the obtained AB.

Experiments were carried out to test the performance of ABNet using different types of images. The experimental results consistently show that ABNet has high classification accuracy. When compared with traditional supervised classifiers (MD, GML, and BPNN) and the previous artificial immune classifiers (MVINC and RLCRSI), ABNet has consistently demonstrated its better overall performance, even though ABNet is not necessarily superior than other classifiers in per-class classification accuracy. McNemar's tests suggest that ABNet is significantly different compared to other classifiers, with the McNemar value above the critical value $\chi^2_{(0.05,1)}$ (3.841459). Comparison among three artificial immune classifiers indicates that MVINC requires less computation time than ABNet and RLCRSI, but its classification accuracy is lower, particularly for AVIRIS hyperspectral image. Being similar to ABNet, RLCRS was also inspired by the biological immune mechanism and has high classification accuracy. However, RLCRSI needed more user-defined parameters to control the classification results, such as stimulation threshold, total resource, and ATS. In contrast, ABNet can adaptively build up the network and guarantee its convergence. This demonstrates that the proposed algorithm is not only able to classify multi-/hyperspectral remote sensing images but also a very competent classifier for processing high volumes of data. Consequently, ABNet provides an effective option for remote sensing image classification. In our future work, we will investigate the method to decrease the number of unclassified antigens which are not recognized by any artificial antibody in the trained ABNet, for example, kernel covering algorithms [51]. In addition, we plan to enhance our classifiers by considering feature selection or extraction using other AIS models in high-dimensional feature space to avoid the Hughes phenomena [52].

ACKNOWLEDGMENT

The authors would like to thank the associate editor and anonymous reviewers for their helpful comments and suggestions and also the research group supervised by Prof. D. Landgrebe, Purdue University, West Lafayette, IN, for providing the free downloads of the AVIRIS Image.

REFERENCES

[1] R. Nishii and S. Eguchi, "Supervised image classification by contextual adaboost based on posteriors in neighborhoods," *IEEE Trans. Geosci. Remote Sens.*, vol. 43, no. 11, pp. 2547–2554, Nov. 2005.
[2] J. B. Campbell, *Introduction to Remote Sensing*. London, U.K.: Taylor & Francis, 2000.
[3] D. Stathakis and A. Vasilakos, "Comparisons of computational intelligence based classification techniques for remotely sensed optical image classification," *IEEE Trans. Geosci. Remote Sens.*, vol. 44, no. 8, pp. 2305–2318, Aug. 2006.
[4] R. O. Duda, P. E. Hart, and D. G. Stork, "*Pattern Classification*," 2nd ed. New York: Wiley, 2001.
[5] J. A. Richards and X. P. Jia, *Remote Sensing Digital Image Analysis, an Introduction*, 3rd revised and enlarged ed. Berlin, Germany: Springer-Verlag, 1999.
[6] F. A. Kruse, A. B. Lefkoff, J. B. Boardman, K. B. Heidebrecht, A. T. Shapiro, P. J. Barloon, and A. F. H. Goetz, "The spectral image processing system (SIPS)—Interactive visualization and analysis of imaging spectrometer data," *Remote Sens. Environ.*, vol. 44, no. 2/3, pp. 145–163, May/Jun. 1993.
[7] L. Samaniego, A. Bárdossy, and K. Schulz, "Supervised classification of remotely sensed imagery using a modified k-NN technique," *IEEE Trans. Geosci. Remote Sens.*, vol. 46, no. 7, pp. 2112–2125, Jul. 2008.
[8] D. E. van de Vlag and A. Stein, "Incorporating uncertainty via hierarchical classification using fuzzy decision trees," *IEEE Trans. Geosci. Remote Sens.*, vol. 45, no. 1, pp. 237–245, Jan. 2007.
[9] T. R. Tooke, N. C. Coops, N. R. Goodwin, and J. A. Voogt, "Extraction urban vegetation characteristics using spectral mixture analysis and decision

tree classifications," *Remote Sens. Environ.*, vol. 113, no. 2, pp. 398–407, Feb. 2009.

[10] J. F. Mas and J. J. Flores, "The application of artificial neural networks to the analysis of remotely sensed data," *Int. J. Remote Sens.*, vol. 29, no. 3, pp. 617–663, Feb. 2008.

[11] F. Ratle, G. Camps-Valls, and J. Weston, "Semisupervised neural networks for efficient hyperspectral image classification," *IEEE Trans. Geosci. Remote Sens.*, vol. 48, no. 5, pp. 2271–2282, May 2010.

[12] G. A. Carpenter, M. N. Gjaja, S. Gopal, and C. E. Woodcock, "ART neural networks for remote sensing: Vegetation classification from Landsat TM and terrain data," *IEEE Trans. Geosci. Remote Sens.*, vol. 35, no. 2, pp. 308–325, Mar. 1997.

[13] W. G. Liu, K. C. Seto, E. Y. Wu, S. Gopal, and C. E. Woodcock, "ARTMMAP: A neural network approach to subpixel classification," *IEEE Trans. Geosci. Remote Sens.*, vol. 42, no. 9, pp. 1976–1983, Sep. 2004.

[14] S. Bandyopadhyay and S. K. Pal, "Pixel classification using variable string genetic algorithms with chromosome differentiation," *IEEE Trans. Geosci. Remote Sens.*, vol. 39, no. 2, pp. 303–308, Feb. 2001.

[15] X. Liu, X. Li, L. Liu, and J. He, "An innovative method to classify remote-sensing image using ant colony optimization," *IEEE Trans. Geosci. Remote Sens.*, vol. 46, no. 12, pp. 4198–4208, Dec. 2008.

[16] J. Muñoz-Marí, F. Bovolo, L. Gómez-Chova, L. Bruzzone, and G. Camps-Valls, "Semisupervised one-class support vector machines for classification of remote sensing data," *IEEE Trans. Geosci. Remote Sens.*, vol. 48, no. 8, pp. 3188–3197, Aug. 2010.

[17] F. Melgani and L. Bruzzone, "Classification of hyperspectral remote sensing images with support vector machines," *IEEE Trans. Geosci. Remote Sens.*, vol. 42, no. 8, pp. 1778–1790, Aug. 2004.

[18] B. Waske and J. A. Benediktsson, "Fusion of support vector machines for classification of multisensor data," *IEEE Trans. Geosci. Remote Sens.*, vol. 45, no. 12, pp. 3858–3866, Dec. 2007.

[19] D. Dasgupta, *Artificial Immune Systems and Their Applications*. Berlin, Germany: Springer-Verlag, 1999.

[20] L. N. de Castro and J. Timmis, *Artificial Immune Systems: A New Computational Intelligence Approach*. London, U.K.: Springer-Verlag, 2002.

[21] M. Pal, "Artificial immune-based supervised classifier for land-cover classification," *Int. J. Remote Sens.*, vol. 29, no. 8, pp. 2273–2291, Apr. 2008.

[22] Y. Zhong, L. Zhang, B. Huang, and P. Li, "An unsupervised artificial immune classifier for multi/hyperspectral remote sensing imagery," *IEEE Trans. Geosci. Remote Sens.*, vol. 44, no. 2, pp. 420–431, Feb. 2006.

[23] L. Zhang, Y. Zhong, B. Huang, and P. Li, "A resource limited artificial immune system algorithm for supervised classification of multi/hyper-spectral remote sensing imagery," *Int. J. Remote Sens.*, vol. 28, no. 7, pp. 1665–1686, Jan. 2007.

[24] Y. Zhong, L. Zhang, J. Gong, and P. Li, "A supervised artificial immune classifier for remote-sensing imagery," *IEEE Trans. Geosci. Remote Sens.*, vol. 45, no. 12, pp. 3957–3966, Dec. 2007.

[25] A. Secker, A. A. Freitas, and J. Timmis, "AISIID: An artificial immune system for interesting information discovery on the web," *Appl. Soft Comput.*, vol. 8, no. 2, pp. 885–905, Mar. 2008.

[26] J. Timmis, A. Hone, T. Stibor, and E. Clark, "Theoretical advances in artificial immune systems," *Theor. Comput. Sci.*, vol. 403, no. 1, pp. 11–32, Aug. 2008.

[27] J. Galeano, A. Veloza, and F. González, "A comparative analysis of artificial immune network models," in *Proc. GECCO*, 2005, pp. 361–368.

[28] L. N. De Castro and F. J. Von Zuben, "An evolutionary immune network for data clustering," in *Proc. IEEE SBRN*, Rio de Janerio, Brazil, 2000, pp. 84–89.

[29] J. Timmis and M. Neal, "A resource limited artificial immune system for data analysis," *Knowl. Based Syst.*, vol. 14, no. 3, pp. 121–130, Jun. 2001.

[30] O. Nasraoui, F. Gonzalez, C. Cardona, C. Rojas, and D. Dasgupta, "A scalable artificial immune system model for dynamic unsupervised learning," in *Proc. GECCO*, 2003, pp. 219–230.

[31] H. Xiong and C. Sun, "Artificial immune network classification algorithm for fault diagnosis of power transform," *IEEE Trans. Power Del.*, vol. 22, no. 2, pp. 930–935, Apr. 2007.

[32] F. Campelo, F. G. Guimaraes, and H. Igarashi, "Multiobjective optimization using compromise programming and an immune algorithm," *IEEE Trans. Magn.*, vol. 44, no. 6, pp. 982–985, Jun. 2008.

[33] T. Stibor and J. Timmis, "An investigation on the compression quality of aiNet," in *Proc. IEEE Symp. Found. Comput. Intell.*, 2007, pp. 495–502.

[34] F. Campelo, F. G. Guimaraes, H. Igarashi, J. A. Ramirez, and S. Noguchi, "A modified immune network algorithm for multimodal electromagnetic problems," *IEEE Trans. Magn.*, vol. 42, no. 4, pp. 1111–1114, Apr. 2006.

[35] N. K. Jerne, "The immune system," *Sci. Amer.*, vol. 229, no. 1, pp. 51–60, 1973.

[36] L. N. De Castro and F. J. Von Zuben, "Learning and optimization using the clonal selection principle," *IEEE Trans. Evol. Comput.*, vol. 6, no. 3, pp. 239–250, Jun. 2002.

[37] G. P. Coelho and F. J. Von Zuben, "Omni-aiNet: An immune-inspired approach for omni optimization," in *Proc. ICARIS*, 2006, pp. 294–308.

[38] N. K. Jerne, "Towards a network theory of the immune system," *Annu. Immunol.*, vol. 125c, pp. 51–60, 1974.

[39] D. E. Rumelhart and J. L. McClelland, *Parallel Distributed Processing*, vol. 1, 2. Cambridge, MA: MIT Press, 1986.

[40] L. Zhang and B. Zhang, "A geometrical representation of McCulloch-Pitts neural model and its applications," *IEEE Trans. Neural Netw.*, vol. 10, no. 4, pp. 925–929, Jul. 1999.

[41] Q. McNemar, "Note on the sampling error of the difference between correlated proportions or percentages," *Psychometrika*, vol. 12, no. 2, pp. 153–157, Jun. 1947.

[42] O. Debeir, I. Van den Steen, P. Latinne, P. Van Ham, and E. Wolff, "Textural and contextual land-cover classification using single and multiple classifier systems," *Photogramm. Eng. Remote Sens.*, vol. 68, no. 6, pp. 597–606, Jun. 2002.

[43] E. Alpaydin, *Introduction to Machine Learning*. Cambridge, MA: MIT Press, Oct. 2004.

[44] J. De Leeuw, H. Jia, L. Yang, X. Liu, K. Schmidt, and A. K. Skidmore, "Comparing accuracy assessments to infer superiority of image classification methods," *Int. J. Remote Sens.*, vol. 27, no. 1, pp. 223–232, Jan. 2006.

[45] P. D. Heermann and N. Khazenie, "Classification of multispectral remote sensing data using a back-propagation neural network," *IEEE Trans. Geosci. Remote Sens.*, vol. 30, no. 1, pp. 81–88, Jan. 1992.

[46] P. F. Hsieh and D. Landgrebe, "Classification of high dimensional data," Ph.D. dissertation, School Elect. Comput. Eng., Purdue Univ., West Lafayette, IN, 1998.

[47] G. F. Hughes, "On the mean accuracy of statistical pattern recognizes," *IEEE Trans. Inf. Theory*, vol. IT-14, no. 1, pp. 55–63, Jan. 1968.

[48] P. Zhong and R. Wang, "Learning conditional random fields for classification of hyperspectral images," *IEEE Trans. Image Process.*, vol. 19, no. 7, pp. 1890–1907, Jul. 2010.

[49] B. Demir and S. Erturk, "Hyperspectral image classification using relevance vector machines," *IEEE Geosci. Remote Sens. Lett.*, vol. 4, no. 4, pp. 586–590, Oct. 2007.

[50] B. Guo, S. R. Gunn, R. I. Damper, and J. D. B. Nelson, "Band selection for hyperspectral image classification using mutual information," *IEEE Geosci. Remote Sens. Lett.*, vol. 3, no. 4, pp. 522–526, Oct. 2006.

[51] W. Zhou, Y. Xu, L. Wang, L. Zhang, and Y. Tan, "A modified constructive neural networks and its application for large-scale data mining," in *Proc. 3rd ICNC*, 2007, pp. 24–28.

[52] L. Zhang, Y. Zhong, B. Huang, J. Gong, and P. Li, "Dimensionality reduction based on clonal selection for hyperspectral imagery," *IEEE Trans. Geosci. Remote Sens.*, vol. 45, no. 12, pp. 4172–4186, Dec. 2007.

Yanfei Zhong (M'11) received the B.S. degree in information engineering and the Ph.D. degree in photogrammetry and remote sensing from Wuhan University, Wuhan, China, in 2002 and 2007, respectively.

In 2007, he joined the State Key Laboratory of Information Engineering in Surveying, Mapping and Remote Sensing, Wuhan University, as an Assistant Professor, where has been a Professor since 2010. His research interests are in multi- and hyperspectral remote sensing image processing, artificial intelligence, and pattern recognition.

Dr. Zhong was a Referee of the IEEE TRANSACTIONS ON SYSTEMS, MAN AND CYBERNETICS—PART B and Pattern Recognition. He was the recipient of the National Excellent Doctoral Dissertation Award of China (2009) and New Century Excellent Talents in University of China (2009).

Liangpei Zhang (M'06–SM'08) received the B.S. degree in physics from Hunan Normal University, Changsha, China, in 1982, the M.S. degree in optics from the Xi'an Institute of Optics and Precision Mechanics, Chinese Academy of Sciences, Xi'an, China, in 1988, and the Ph.D. degree in photogrammetry and remote sensing from Wuhan University, Wuhan, China, in 1998.

He is currently with the State Key Laboratory of Information Engineering in Surveying, Mapping and Remote Sensing, Wuhan University, as the Head of the Remote Sensing Division. He is also a "Chang-Jiang Scholar" Chair Professor appointed by the Ministry of Education, China. He has more than 200 research papers and is the holder of five patents. He is currently a Principal Scientist for the China State Key Basic Research Project (2011–2016) appointed by the Ministry of National Science and Technology of China to lead the remote sensing program in China. His research interests include hyperspectral remote sensing, high-resolution remote sensing, image processing, and artificial intelligence.

Dr. Zhang is a fellow of IEE, executive member (Board of Governor) of the Chinese National Committee of International Geosphere–Biosphere Programme, executive member for China Society of Image and Graphics, and others. He regularly serves as a Cochair of the series SPIE Conferences on Multispectral Image Processing and Pattern Recognition, Conference on Asia Remote Sensing, and many other conferences. He is an Editor of several conference proceedings, issues, and the Geoinformatics Symposiums. He also serves as an Associate Editor of the *International Journal of Ambient Computing and Intelligence*, *International Journal of Image and Graphics*, *International Journal of Digital Multimedia Broadcasting*, *Journal of Geospatial Information Science*, and *Journal of Remote Sensing*.